SUPPLEMENTARY MATERIALS

Table 1A: Characteristics of the different images used in the image registration procedure.

	In-vivo **Axial**	***In-vivo*** **Coronal**	***In-vivo*** **Sagittal**	***Ex-vivo*** **Axial**	**Histopathology (in MICE)**	**Registered histopathology**
Repetition time (ms)	9946	6133	5793	2500	-	-
Echo time (ms)	103	128	128	117	-	-
Flip angle (°)	125	111	111	111	-	-
Number of averages (NEX)	1	3	3	15	-	-
Slice thickness (mm)	2.5	3	3	5	5×10^{-3}	2.5
In-plane pixel size (mm^2)	0.410 x 0.410	0.469 x 0.469	0.469 x 0.469	0.195 x 0.195	0.015 x 0.015	0.1 x 0.1
Matrix size	512 x 512	512 x 512	512 x 512	512 x 512	3840 x 1960	2101 x 2101

Table 2A: In-plane error (mm) of group 1 (14 patients with extraprostatic surgical margins) and group 2 (11 patients without extraprostatic surgical margins).

	Min	**1st Qu.**	**Median**	**Mean**	**3dr Qu.**	**Max**	**SD**
Group 1 (before deformable registration)	0. 2	1.4	2.1	2.3	3.2	4.4	1.8
Group 1 (after deformable registration)	0.4	1.2	1.8	2.0	2.6	4.8	1.1
Group 2 (before deformable registration)	0.1	0.9	1.3	1.7	2.4	4.8	1.2
Group 2 (after deformable registration)	0.2	1.0	1.5	1.7	2.5	4.3	1.0

Table 3A: Summary of other publications performing co-registration of histopathology to *in-vivo* MRI and determine their method uncertainty based on comparing positions of landmarks.

Publication	Registrations scheme	Evaluation method	Uncertainty
Ward et al (2012) [1]	Landmarks-based (by extrinsic fiducial markers) comparing rigid and nonrigid thin-plate spline registration of histopathology to *in-vivo* MRI.	Euclidian distance between corresponding manually determined landmarks in the *in-vivo* T2w MRI and registered histopathology sections.	2.3 ± 1.7 mm (rigid) 1.1 ± 0.7 mm (nonrigid)
Orczyk et al (2012) [2]	Landmark-based (by extrinsic fiducial markers) spatial registration (rigid and affine) of histopathology to *in-vivo* MRI.	The mean root square distance across corresponding control points defined in the registered histopathology and *in-vivo* MRI.	2.89 mm (rigid) 1.59 mm (affine)
Kalavagunta et al (2015) [3]	Local affine transformation assisted by internal structures (IS) of histopathology to *in-vivo* MRI.	Root mean squared distance between manually detected landmarks (independent from the ones used in the registration) defined in the *in-vivo* MRI and the native histopathology before transformed.	1.54 ± 0.64 mm (with IS) 2.92 ± 1.76 mm (without IS)
Reynolds et al (2015) [4]	Initial alignment followed by a deformable registration of *in-vivo* MRI to *ex-vivo* MRI. Histopathology to *ex-vivo* MRI by a rigid registration followed by an initial control point alignment and automatic registration using similarity transform.	Mean distance between point features. Quantitative assessment by computing the mean distance between control points after registration.	3.2 ± 1.3 mm 0.57 ± 0.28 (0.06–1.99) mm
Uribe et al (2015) [5]	An affine and a nonrigid transform of the *in-vivo* MRI to histopathology. The nonrigid was used to correct for deformation due to the usage of endorectal coil during *in-vivo* MRI.	Median distance between corresponding landmarks in the *in-vivo* MRI and registered histopathology sections.	1.55 (0.3-3.1) mm
Dinh et al (2017) [6]	Deformable registration method based on selected landmarks.	Average distance between landmark in the *in-vivo* MRI and registered histopathology.	2.1 mm (dataset 1) 2.6 mm (dataset 2)
Li et al (2017) [7]	Multi-scale spectral embedding registration of histopathology to *in-vivo* MRI.	Root mean square distance between corresponding landmarks in registered histopathology and *in-vivo* MRI.	2.96 ± 0.76 mm

REFERENCES

1. Ward AD, Crukley C, McKenzie CA, Montreuil J, Gibson E, Romagnoli C, et al. Prostate: registration of digital histopathologic images to in vivo MR images acquired by using endorectal receive coil. Radiology. 2012;263:856–864. http://www.ncbi.nlm.nih.gov/pubmed/22474671.
2. Orczyk C, Mikheev A, Rosenkrantz A, Melamed J, Taneja SS, Rusinek H. Imaging of prostate cancer: a platform for 3D co-registration of in-vivo MRI ex-vivo MRI and pathology. Proc SPIE-the Int Soc Opt Eng. 2012;8316:1–18. http://proceedings.spiedigitallibrary.org/proceeding.aspx?doi=10.1117/12.911369.
3. Kalavagunta C, Zhou X, Schmechel SC, Metzger GJ. Registration of in vivo prostate MRI and pseudo-whole mount histology using Local Affine Transformations guided by Internal Structures (LATIS). J Magn Reson Imaging. 2015;41:1104–1114.
4. Reynolds HM, Williams S, Zhang A, Chakravorty R, Rawlinson D, Ong CS, et al. Development of a registration framework to validate MRI with histology for prostate focal therapy. Med Phys. 2015;42:7078–7089.
5. Uribe CF, Jones EC, Chang SD, Goldenberg SL, Reinsberg SA, Kozlowski P. In vivo 3T and ex vivo 7T diffusion

tensor imaging of prostate cancer: Correlation with histology. Magn Reson Imaging. 2015;33:577–583. http://www.ncbi.nlm.nih.gov/pubmed/25721995.
6. Dinh CV, Steenbergen P, Ghobadi G, Poel H Van Der, Stijn WTPJ. Multicenter validation of prostate tumor localization using multiparametric MRI and prior knowledge. Med Phys. 2017;44:949–961. http://ovidsp.ovid.com/ovidweb.cgi?T=JS&PAGE=reference&D=emexa&NEWS=N&AN=615061982.
7. Li L, Pahwa S, Penzias G, Rusu M, Gollamudi J, Viswanath S, et al. Co-Registration of ex vivo Surgical Histopathology and in vivo T2 weighted MRI of the Prostate via multi-scale spectral embedding representation. Sci Rep. 2017;7:1–12. http://dx.doi.org/10.1038/s41598-017-08969-w.

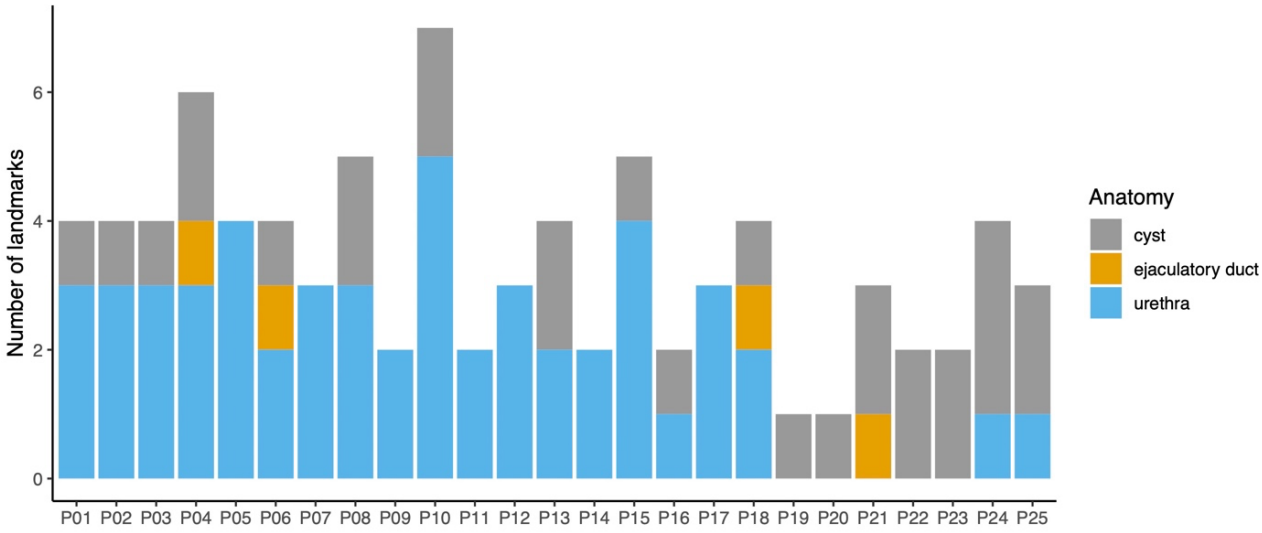

Figure 1A: Identified landmarks per patients and their anatomical location.